Journal of Molecular Liquids 397 (2024) 124057

Contents lists available at ScienceDirect

Journal of Molecular Liquids

journal homepage: www.elsevier.com/locate/molliq

Investigating the efficacy of functionalized graphene oxide with polyhedral oligomeric silsesquioxane as an effective additive in sustainable ionic liquid-based electrolytes for dye-sensitized solar cells through experimental and DFT studies

Shiva Orangi [a], Elaheh Kowsari [a,*], Mohammad Mohammadizadeh Boghrabad [a], Saeedeh Sarabadani Tafreshi [a], Seeram Ramakrishna [b,*], Mahboobeh Rafieepoor Chirani [a], Amutha Chinnappan [b], Nora H. de Leeuw [c,d]

[a] Department of Chemistry, Amirkabir University of Technology, No. 424, Hafez Avenue, 1591634311 Tehran, Iran
[b] Department of Mechanical Engineering, Center for Nanofibers and Nanotechnology, National University of Singapore 119260, Singapore
[c] School of Chemistry, University of Leeds, LT2 9JT Leeds, UK
[d] Department of Earth Sciences, Utrecht University, 3584 CB Utrecht, the Netherlands

ARTICLE INFO

Keywords:
Functionalized graphene oxide
Ionic liquids
Environmentally sustainable nanocomposite electrolytes
Density functional theory
Dye-sensitized solar cells

ABSTRACT

The focus of the study has been on the first-ever use of functionalized graphene oxide with polyhedral oligomeric silsesquioxane (FGO-POSS) as an effective additive to ionic liquid-based electrolytes in dye-sensitized solar cells (DSSCs). The electrolytes consisted of binary ionic liquids (ILs), 1-ethyl-3-methylimidazolium iodide (EMII), and 1-butyl-3-methylimidazolium iodide (BMII). Different concentrations of the efficient additive FGO-POSS, ranging from 0% to 1%, were incorporated into the electrolytes.

Under highly controlled conditions, a series of reactions was conducted to synthesize FGO-POSS. By reacting graphene oxide (GO) with L-phenylalanine, initially, GO-L-phenylalanine was obtained. In the next phase, GO-L-Phenylalanine reacted with SSQ-[3-(2-Aminoethyl) amino] propyl-Heptaisobutyl substituted to modify its structure with polyhedral oligomeric silsesquioxane (POSS). The ILs, namely EMII, and BMII, were synthesized using the scientific methodologies detailed in the referenced articles. Furthermore, BMII was functionalized with CuI ($BMICuI_2^-$) through a specific procedure.

Five types of electrolytes were prepared to be employed in DSSCs using prepared ILs and FGO-POSS, and their results were reported to show the electrical and gelatin features of these types of electrolytes. According to this study's findings, using FGO-POSS as an innovative and efficient additive in ILs-based environmentally sustainable nanocomposite electrolytes in an amount of 0.75 wt% increased the value of the short circuit current density (J_{SC}) from 9.433 mA.cm^{-2} to 15.592 mA.cm^{-2}, the open circuit voltage (V_{OC}) from 0.738 V to 0.762 V, and the overall efficiency (η) increased from 4.965 to 8.303 %. The FGO-POSS and ILs, EMII, and $BMICuI_2^-$ boost electron transport and electrolyte conductivity, resulting in increased J_{SC}, V_{OC}, and η. Results of the density functional theory (DFT) calculation indicated that the adsorption of the FGO-POSS electrolyte additives on the TiO_2 electrode surface produces midgap states in the band gap of TiO_2, resulting in the reduction of the total bandgap and less barrier electron transfer and a redshift in the adsorption edge and enhancement of DSSCs' efficiency.

1. Introduction

In recent years, solar energy has grown in popularity as a source of energy. Many regions of the world have access to abundant, sustainable, and clean solar energy [1–6]. Future energy supplies depend on photovoltaic technologies made from inexpensive, eco-friendly raw materials, and dye-sensitized solar cells (DSSCs) have lately been receiving plenty of scientific interest owing of their simple manufacturing procedures and comparatively high power conversion efficiency (PCE) [7–11]. Since being proposed by Gratzel and O'Regan

* Corresponding authors.
E-mail addresses: Kowsarie@aut.ac.ir (E. Kowsari), seeram@nus.edu.sg (S. Ramakrishna).

https://doi.org/10.1016/j.molliq.2024.124057
Received 11 August 2023; Received in revised form 22 November 2023; Accepted 11 January 2024
Available online 23 January 2024

in 1991, DSSCs have attracted academic and industry interest [12]. In comparison to traditional silicon solar cells, DSSCs exhibit better efficiency, reduced manufacturing costs, more straightforward fabrication, and operation that is considerably more ecologically friendly [13,14]. According to a recent study, developing DSSCs allows for achieving a 15.2 % PCE under normal circumstances [15]. A DSSC typically consists of three essential parts: an electrolyte, a dye-sensitized TiO_2 electrode (anode), and a Pt counter electrode (cathode). In the DSSC, excited electrons from the molecules of dye adsorbed on the layer of TiO2 are transferred to the photoanode's conduction band. The excited dye molecules are regenerated by the oxidation and reduction process of I^-/I_3^-, a redox pair, inside the electrolyte environment following the move of the electron to the counter electrode and subsequent entrance of the electron into the electrolyte environment [16]. Although many aspects go into maintaining DSSCs at their best possible performance, a suitable electrolyte system composition with interaction at the same time of the electrolyte, anode, and cathode is considered especially crucial [17,18]. Organic solvent-based liquid electrolyte leakage is still an issue, which prevents their use for extensive commercialization [16,19]. To get around the problems with liquid electrolytes, significant research has been put into developing alternatives to electrolytes that are based on organic solvents, including ionic liquid-based electrolytes, p-type semiconductors, and gel polymer electrolytes [20–22]. Ionic liquids (ILs) at room temperature, particularly those based on imidazolium cations, have been studied as potential substitutes for liquid electrolytes formed by organic solvents and have demonstrated promising outcomes [23–29]. They are a green and sustainable option to be utilized as electrolytes in DSSC applications due to their unique characteristics, which have a high ionic conductivity, a broad electrochemical potential window, a low vapor pressure, and a significant degree of thermal stability. Also, the presence of transition metals adjacent to ionic liquids in the form of salts can enhance their properties and raise the conductivity within the electrolyte [30,31]. Additionally, the usage of materials including polyionic liquids (PIL) with ILs and ethylene carbonate (EC) in the electrolyte of DSSCs has been shown to provide positive outcomes [32]. Using ionic liquids rather than liquid electrolytes based on organic solvents minimizes electrolyte leakage but lowers DSSC efficiency, restricting this type of solar cell's commercialization. According to specific research, using carbon-based materials in electrolytes can result in highly efficient cells for DSSC applications [17,33,34]. Due to its exceptional physicochemical features, theoretically high surface-to-volume ratio, superb theoretically particular mechanics, and extraordinary electronic properties, graphene has emerged as a promising material among carbon-based ones [35–38]. About graphene, graphene oxide (GO) has the capacity for chemical modification as a result of its unique properties and functional groups like epoxy, hydroxyl, and carboxylic acid [39–41]. Enhancing the dispersion quality of graphene by functionalization with additional elements can change its electrical characteristics, narrow its bandgap, and make it more useful for device applications [42–46]. Due to their properties, phenyl compounds, particularly those with nitrogen in their structure, can be a desirable choice for functionalizing and strengthening graphene oxide, among other substances [47–50]. An activation zone with electrocatalytic capabilities for the I^-/I_3^- redox process could potentially be produced by functionalizing nitrogen-enriched GO sheets, which would alter the charge distribution of carbon atoms adjacent to nitrogen [51]. In addition, GO becomes more amorphous after being functionalized with polyhedral oligomeric silsesquioxane (POSS), which enhances the filling of electrolytes in TiO_2 pores without needing a crystal growth inhibitor. POSS's presence in the structure of graphene oxide boosts the electrolyte's effectiveness because of its characteristics and the effect it has when combined with ionic liquids, making it a suitable addition for electrolytes based on ionic liquids [52–54].

According to the explanations, one form of the electrolyte was developed based on binary ionic liquids in this study work employing two types of ionic liquids, namely 1-ethyl-3-methylimidazolium iodide (EMII) and 1-butyl-3-methylimidazolium iodide functionalized with CuI ($BMICuI_2^-$). We investigated the impact of this effective additive on the functionality of the studied electrolyte and the efficiency of the DSSC by synthesizing functionalized GO with POSS compounds and employing them as potential effective additives for electrolytes based on ionic liquids. Using density functional theory (DFT) computations, we also investigated how functionalized graphene oxide with polyhedral oligomeric silsesquioxane (FGO-POSS) affected electron transport in DSSCs. Along with GO's electrocatalytic properties, the nitrogen atoms in the functionalized GO structure cause electron tunneling in the ILs matrix. Additionally, the presence of the POSS component in the structure of GO works as a stimulant for electron transfers because of its properties and unique molecular structure, which eventually enhances the electrocatalytic performance of GO. In general, the turning point and appeal of this study may be attributed to the improvement in conversion efficiency attained in DSSCs when adding the novel effective additive FGO-POSS in the structure of electrolytes based on EMII and $BMICuI_2^-$ ionic liquids.

2. Experimental

2.1. Materials and chemicals

SSQ-[3-(2-Aminoethyl)amino]propyl-Heptaisobutyl substituted, potassium permanganate ($KMnO_4$), sodium nitrate ($NaNO_3$), 4-*tert*-Butylpyridine (TBP), copper(I) iodide (CuI), ethyl iodide (C_2H_5I), Graphite powder of greater than 99.99 % purity, and butyl iodide (C_4H_9I) were bought from Sigma Aldrich (Milwaukee, WI). Hydrogen peroxide (H_2O_2), thionyl chloride ($SOCl_2$), L-phenylalanine, 1-methylimidazole ($C_4H_6N_2$), hydrochloric acid (HCl), lithium iodide (LiI), Iodine (I_2), sulfuric acid (H_2SO_4), and ethanol were obtained from Merck (Darmstadt, Germany). The chemicals and other solvents utilized in the present study included analytical-grade commercial chemicals.

2.2. Synthesis of $BMICuI_2^-$ and EMII

Under a nitrogen environment, the synthesis of 1-butyl-3-methylimidazolium iodide (BMII) was carried out in a flask with three holes and a strong magnetic stirrer. Under the conditions of a cold water bath, 1-methylimidazole was first added to the flask. Butyl iodide was then gradually added drop by drop (at a molar ratio of 1:1.5), and for 48 h, at 80 °C, the reaction mixture was kept. A viscous orange liquid was produced after it was purified using various novel techniques once it had risen to room temperature. The same molar ratios and circumstances were used to synthesize 1-ethyl-3-methyl-imidazolium iodide (EMII) as well. The BMII ionic liquid was functionalized with CuI after the ionic liquids were prepared. BMII and CuI were reacted in a 1:1 M ratio for 72 h with magnetic stirring in a nitrogen atmosphere at 80 °C to functionalize BMII with CuI. 1-butyl-3-methylimidazolium copper iodide ($BMICuI_2^-$) was produced and subsequently purified. The purification process involved multiple washings with ethyl acetate, followed by placement in a vacuum oven for 24 h [22,44,55].

2.3. Synthesis of GO and FGO-POSS

A modified Hummers method was utilized for synthesizing GO sheets from natural graphite powder [56][William, 1958 #5]. This was done by continually stirring in an ice bath while adding 2 g of graphite and 1.5 g of $NaNO_3$ to 6.75 ml of pure sulfuric acid. After that, 9 g of $KMnO_4$ was added gradually during an hour, and the mixture was stirred in an ice water bath for two hours. After being taken out from the ice bath, heated to around 35 °C, and held for one hour at this temperature. To produce a high-viscosity liquid, 24 h were spent stirring the mixture continually. As the reaction progressed, 200 ml of H_2SO_4 (5 wt% aqueous solution) was gradually added for 1 h. Then, 15 min were spent maintaining a temperature of 98 °C for the mixture. For 2 h, the suspension was agitated. Then, 6 ml of H_2O_2 (30 wt% aqueous solution)

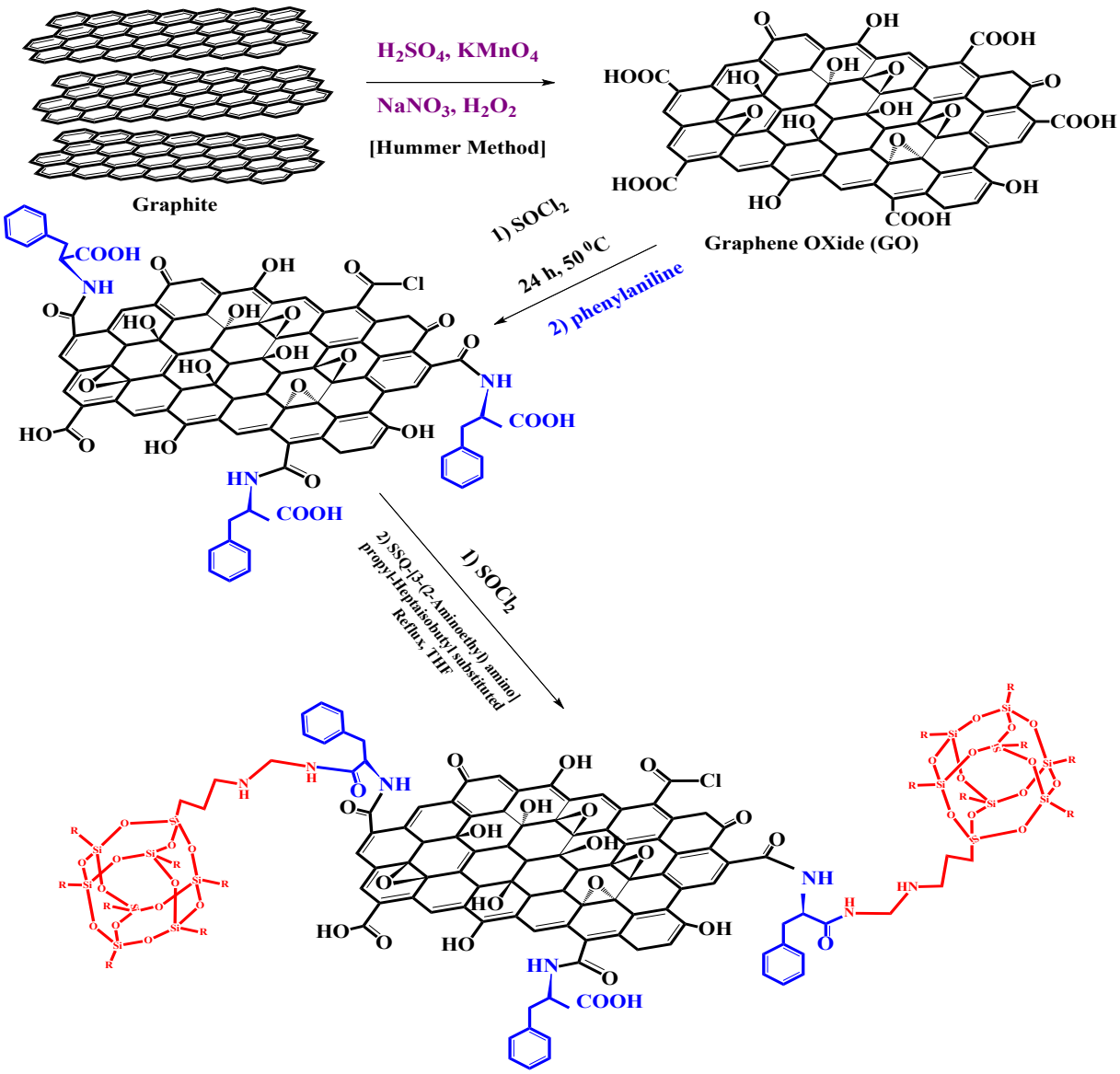

Scheme 1. The procedures involved in synthesizing FGO-POSS.

was added into the mixture to decrease the residual $KMnO_4$ and $KMnO_2$. Following multiple stages of filtering, the resulting mixture was washed with an aqueous solution containing 3 % wt H_2SO_4 and 5 % wt H_2O_2. Deionized water was used for purification as well as acid and salt removal. In the first step, acylation of graphene oxide (GO) was performed, followed by the functionalization of L-Phenylalanine. Subsequently, the GO-L-Phenylalanine functionalized compound was acylated in the subsequent stage.

In the synthesis of FGO-POSS, a 100 ml three-neck round bottom flask equipped with a reflux condenser was used. Into this flask, 2 g of SSQ-[3-(2-Aminoethyl) amino] propyl-Heptaisobutyl substituted and 2 g of acylated GO -L-Phenylalanine functionalized were added. Tetrahydrofuran (15 ml) was used as the solvent throughout the reaction process. The reaction mixture was stirred for a duration of 24 h at a temperature of 50 °C and followed by placement in a vacuum oven for 24 h. The Synthesis steps of GO synthesis and functionalization with POSS are depicted in Schematic 1.

2.4. Standard and nanocomposite electrolyte preparation

Binary ionic liquids of $BMICuI_2$ and EMII were used for preparing the electrolyte. A standard electrolyte was prepared using 1 M EMII, 1 M $BMICuI_2$, 0.1 M LiI, 0.1 M I2, and 0.5 M TBP. To create the four different types of nanocomposite electrolytes, E1, E2, E3, and E4, FGO-POSS was added to the standard electrolyte in weight percentages of 0.25, 0.5, 0.75, and 1. After that, all of the electrolytes were swirled for 24 h at room temperature in the same conditions as on the stirrer. Preparing nanocomposite electrolytes in four different percentages results in ideal comparison conditions for comparing nanocomposite electrolytes to the standard electrolyte.

2.5. Fabrication of DSSCs

Fluorine-doped tin oxide conductive glass (FTO) was used as the experiment's substrate, which served as both the working electrode (photoanode) and the counter electrode (cathode). FTO surface pollutants were washed with soap and water, deionized water, 0.1 M HCl, and deionized water, respectively, in a standard wash. Then, 30 min at 70 °C were spent immersing the FTO glasses in a 40 mM $TiCl_4$ aqueous solution, followed by an ethanol wash. A dye-absorbent layer consisting of TiO_2 paste with 25 nm-sized TiO_2 particles and scattering particles of approximately 400 nm TiO_2 paste were applied to FTO, resulting in a

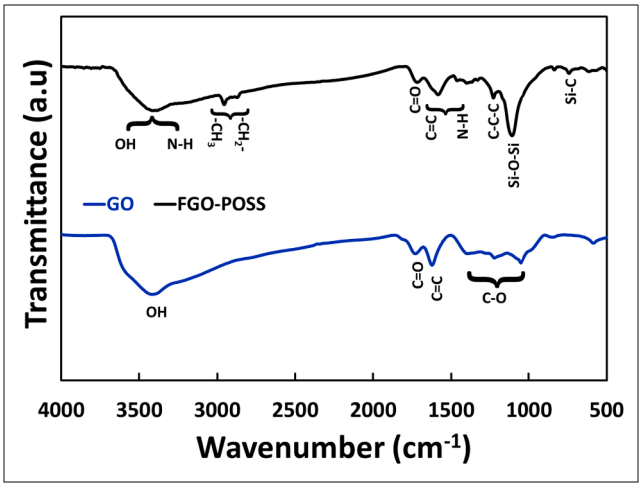

Fig. 1. GO and FGO-POSS's FT-IR spectra.

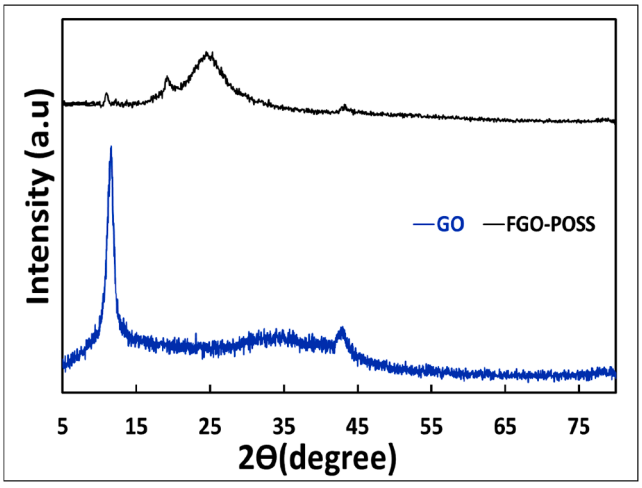

Fig. 2. Patterns of GO and FGO-POSS on the XRD.

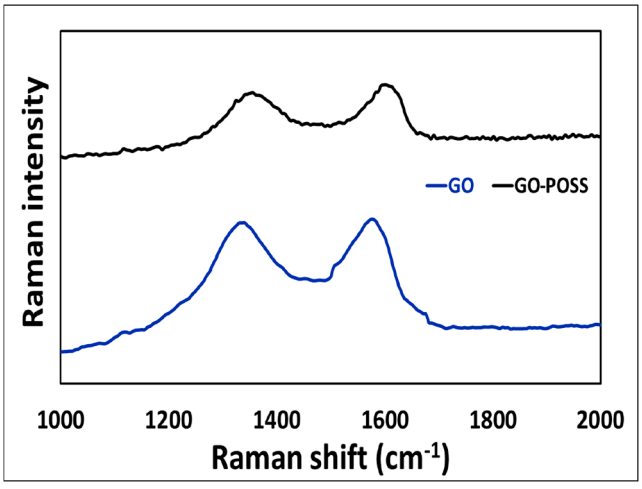

Fig. 3. GO and FGO-POSS corresponding Raman spectra.

0.16 cm^2 area and a thickness of 8 μm, to create the photoanode utilizing the doctor-blade technique. Using a temperature program, the resulting electrodes were heated over a set amount of time from room temperature to 500 °C. They were placed in an aqueous solution containing 40 mM $TiCl_4$ for 30 min at 70 °C before being heated to 500 °C. The photoanodes were submerged at ambient temperature in 0.5 mM N719 (Di-tetrabutylammonium *cis*-bis (isothiocyanato) bis (2, 2′-bipyridyl-4, 4′-dicarboxylato) ruthenium (II)) solution in ethanol and in the dark for 18–24 h to absorb dye molecules. A drop of a 10 mM H_2PtCl_6 solution in ethanol was put over the conductive surface of FTO, which contains a hole with a diameter of 0.6 mm, to create the cathode electrode. This solution was spread evenly across the whole surface of FTO. The cathodes were manufactured after 15 min of heating at 460 °C and gradual cooling to ambient temperature. A Surlyn polymer sheet measuring 7 μm thick links two electrodes. Finally, the electrolyte was injected through the cathode hole by a vacuum pump. With Surlyn film and cover glass, the tiny hole was sealed. The fabrication of DSSCs with standard electrolytes and nanocomposite electrolytes was similar.

2.6. Photovoltaic characterization

The fabricated DSSCs were exposed to device radiation (Sharif Solar, SIM-1000) at an intensity (1000 Wm^{-2}) equivalent to AM 1.5 radiation from 0 to 150 mV, with a step of 10 mV. This allowed for the creation of the J-V diagram using IviumStat.XRe. Through analysis, the photovoltaic properties, VOC, JSC, efficiency (η %), and fill factor (FF) were obtained. IviumStat.XRe and a solar light simulator (Sharif Solar, SIM-1000) were used to obtain the electrochemical impedance spectrum (EIS) of the cells at an AC range of 20 mV in the frequency range of 0.01e100 kHz. Equivalent circuits and Nyquist diagrams were examined using Z-View software.

3. Results and discussion

Due to graphene oxide's distinct characteristics and the inclusion of POSS in its structure, functionalized graphene oxide with POSS (FGO-POSS) has produced an appealing combination. The compound's impressive performance as an innovative and efficient additive in DSSC's ionic liquid-based electrolytes demonstrates the material's potential. This study analyzed and evaluated FGO-POSS as an innovative and efficient additive for DSSC's electrolytes.

3.1. Characterization of GO and FGO-POSS

Fig. 1 depicts the FTIR spectroscopy of GO and FGO-POSS. The stretching OH band was visible in the GO's FTIR spectrum at 3432 cm^{-1}. The band that appeared around 1730 cm^{-1} relates to C = O stretching. Aromatic bonds (C = C stretching) are associated with the band at 1625 cm^{-1}. Oxygenated groups, including the C-O stretching vibrations of epoxy, alcohol, and carboxylic acid groups in GO, have relations to the bands between 1000 and 1400 cm^{-1}. The band seen in the area of 3412 cm^{-1} on the FT-IR spectrum of FGO-POSS is due to OH and N–H stretching vibrations. In FGO-POSS, the CH_2 and CH_3 groups' C–H stretching is represented by the bands at 2878 and 2955 cm^{-1}. Stretching C = O has been associated with the 1718 cm^{-1} band. The comparatively broad band at 1600 cm^{-1} is due to overlapping (C = C stretching and N–H bending) vibrations. The OH bending vibrations are indicated by the band at 1402 cm^{-1}. The bond (C–C–C) caused the band at 1229 cm^{-1} that entered the graphene oxide structure following GO functionalization. The detected band at 1109 cm^{-1} is pertaining to the Si-O-Si group that, following functionalization, joined the network of graphene oxide. The Si-C bond is associated with the band around 745 cm^{-1} [57,58].

To compare the differences between the exfoliation of GO and FGO-POSS, X-ray powder diffraction was performed. Two GO and FGO-POSS samples' XRD spectra in the 2θ range of 5–80° are shown in Fig. 2. The most prominent peak in the XRD patterns of GO occurs at 2θ = 11.63°, demonstrating that the distance between the plates is 7.63 A°. The presence of oxygen agents between the GO plates is responsible for the considerable distance between the plates. The XRD spectral structure is

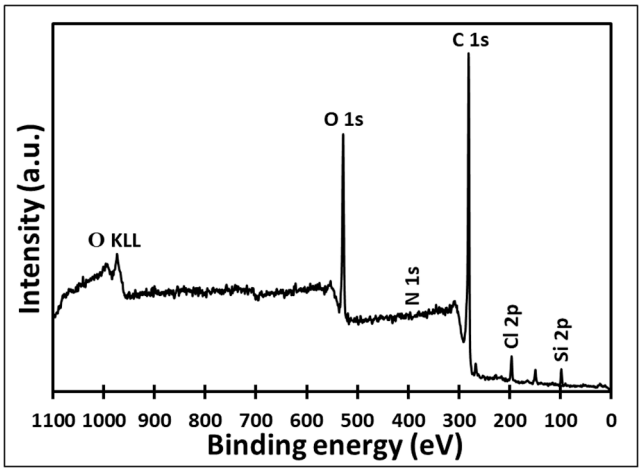

Fig. 4. XPS survey spectrum of the FGO-POSS.

messed up after FGO-POSS, and an amorphous band appears on the spectrum between 2θ =10° and 2θ =30°. This is due to the presence of POSS in the GO structure, which mainly reveals the irregular and amorphous structure and low crystallinity of FGO-POSS. The most prominent FGO-POSS peak came at 2θ =24.69°, indicating that the reduction procedure was successful and that the distance between functionalized graphene oxide (FGO) sheets was reduced by up to 3.86 A° [59,60].

The GO and FGO-POSS Raman spectra are shown in Fig. 3. The two peaks that emerge in the Raman spectrum of GO are the significant properties of GO and are seen in the ranges of 1345 cm^{-1} (D band) and 1585 cm^{-1} (G band).

The D band, which is ascribed to hybridization sp^3, appears by amorphous carbon atoms present in carbon compounds like GO. As opposed to this, the hexagonal structure of GO has hybridized carbon atoms (sp^2) that cause the G band to appear. In contrast, the G band emerges due to the presence of hybridized carbon atoms sp^2 in the hexagonal structure of GO. Raman spectroscopy is another effective method for determining GO functionalization. The difference in the I_d/I_g ratio in the spectra of GO and FGO-POSS can demonstrate the

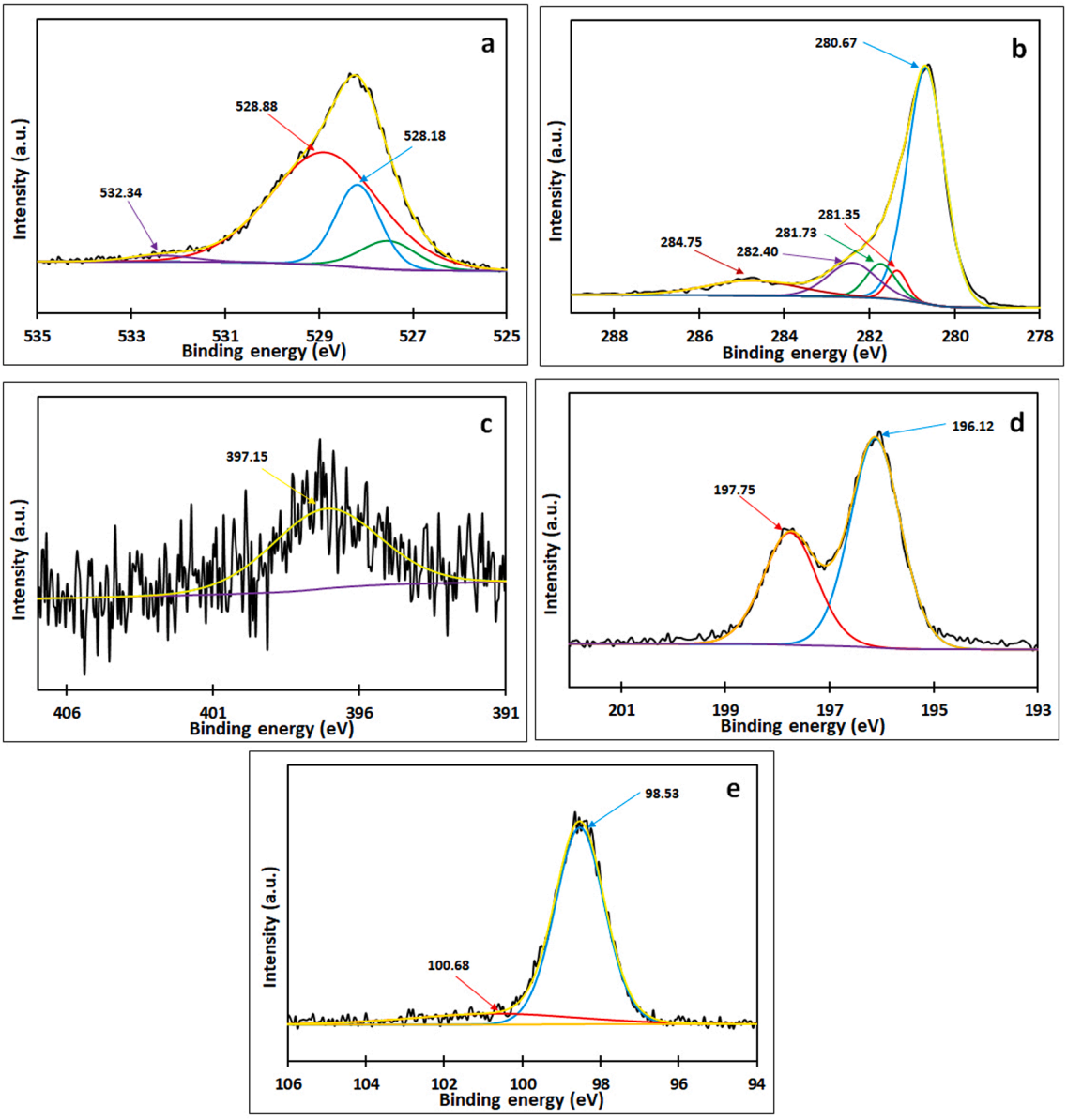

Fig. 5. Deconvolution of high-resolution XPS spectra for the elements in (a) O 1 s, (b) C 1 s, (c) N 1 s, (d) Cl 2p, and (e) Si 2p.

Table 1
Atomic percentage values for the chemical bonds of FGO-POSS obtained from XPS analysis.

Peak	Assignments	Peak position (eV)	Peak area (CPS. eV)	%At.
O 1 s	C = O	527.52	1764.0	8.86
	C-O/C-O-Si	528.17	4094.8	20.57
	Si-O-Si	528.88	13592.2	68.27
	C-O-C	532.34	458.5	2.30
C 1 s	C–C/C = C	280.67	22208.1	65.00
	C-N/Si-C	281.35	1466.6	4.29
	C-O-C	281.73	2607.4	7.63
	C = O	282.40	4261.3	12.47
	O-C = O	284.74	3621.2	10.60
N 1 s	C-N	397.35	439.1	100
Cl 2p	Cl $2p_{3/2}$	196.12	1755.8	63.60
	Cl $2p_{1/2}$	197.76	1005.0	36.40
Si 2p	Si-O-Si	98.53	1286.0	84.31
	Si-C	100.67	239.2	15.69

functionalization of GO with POSS. In the GO's Raman spectra, the I_d/I_g is 0.98, whereas the I_d/I_g in the Raman spectra of FGO-POSS is 0.94. The difference in intensity ratio (I_d/I_g) indicates that GO functionalization was successful. Surface defects in GO have been modified using covalent bonds formed during its functionalization with POSS [61,62].

Fig. 4 depicts the FGO's X-ray photoelectron spectroscopy (XPS). According to Fig. 4, the presence of C 1 s, O 1 s, N 1 s, Si 2p, and Cl 2p peaks confirms the existence of carbon, oxygen, nitrogen, silicon, and chlorine elements in the FGO-POSS. Using CasaXPS software, the atomic percentage values of the oxygen, carbon, nitrogen, silicon, and chlorine elements equal 16.29 %, 76.48 %, 0.45 %, 3.96 %, and 2.82 %, respectively. Fig. 5 showing deconvoluted curves of C 1 s, O 1 s, N 1 s, Si 2p, and Cl 2p of FGO-POSS. Table 1 reports the atomic percentages of the chemical bonds.

Based on Table 1 and Fig. 5, the O 1 s peak can be deconvoluted into four peaks at 527.52, 528.17, 528.88, and 532.34 eV, corresponding to C = O, C-O/C-O-Si, Si-O-Si, and C-O-C bonds, respectively, in the structure of functional graphene oxide and POSS [63]. Also, C 1 s peak is divided into five peaks at 280.67, 281.35, 281.73, 282.40, and 284.74 eV, which are respectively related to C–C/C = C bonds in aromatic rings, C-N/Si-C bonds, C-O-C, and C = O/O-C = O bonds in FGO structures [64]. In addition, the N 1 s peak at 397.35 eV is attributed to the C-N bond in the under-studied sample. Chlorine and silicon elements are also other detected elements in the chemical structure of the material. The Si-O-Si bond at 98.53 eV and Si-C at 100.67 eV prove the covalent bond between the POSS structure and the functionalized graphene oxide nanosheets. The N and Si atoms localized in the functional group can be a promising candidate as an active site for iodine-catalyzed reactions and nanoelectronics systems [65].

In the FGO-POSS field emission scanning electron microscopy (FESEM) images in Fig. 6, the existing wrinkles are the main

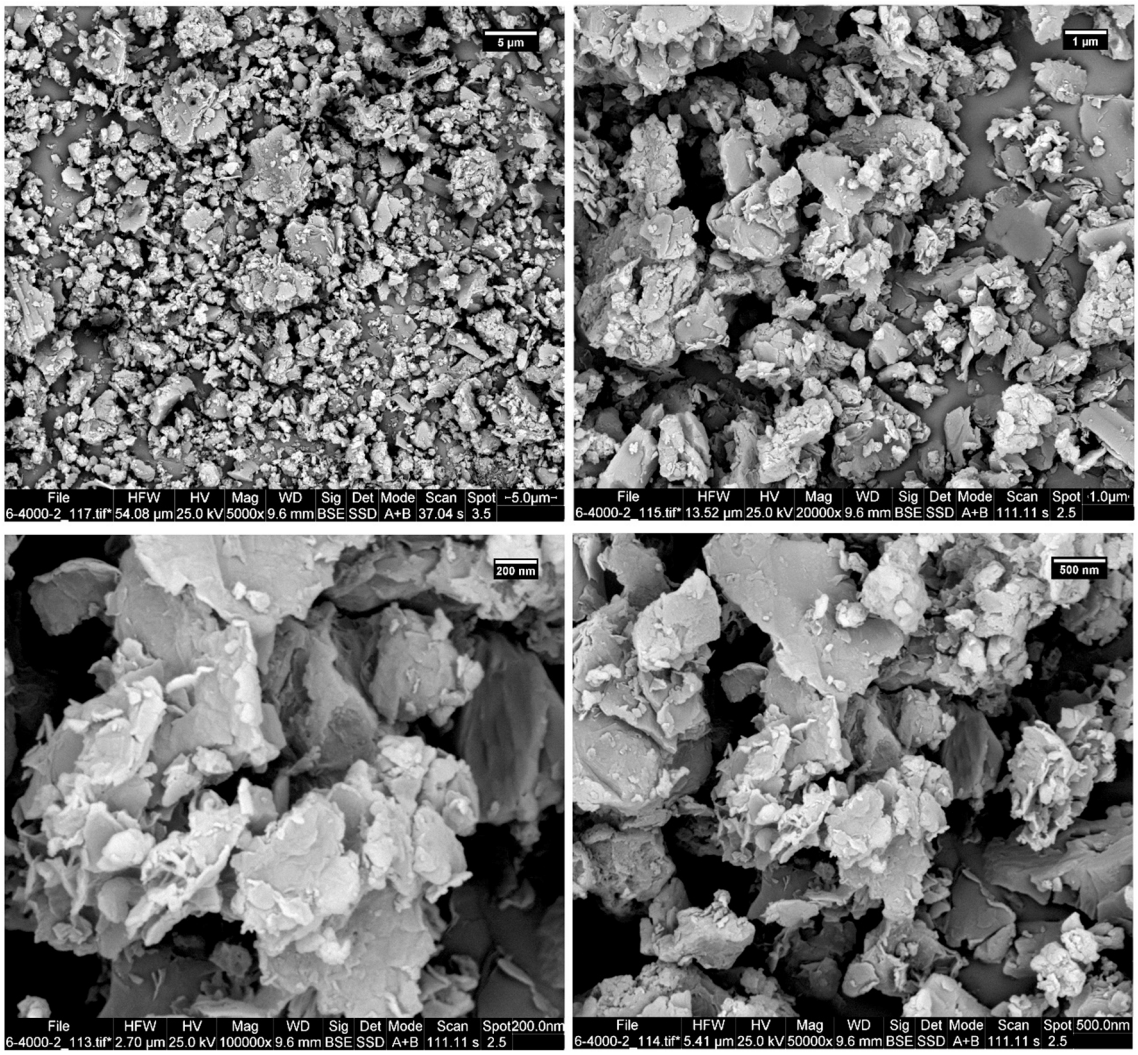

Fig. 6. FESEM image of FGO-POSS.

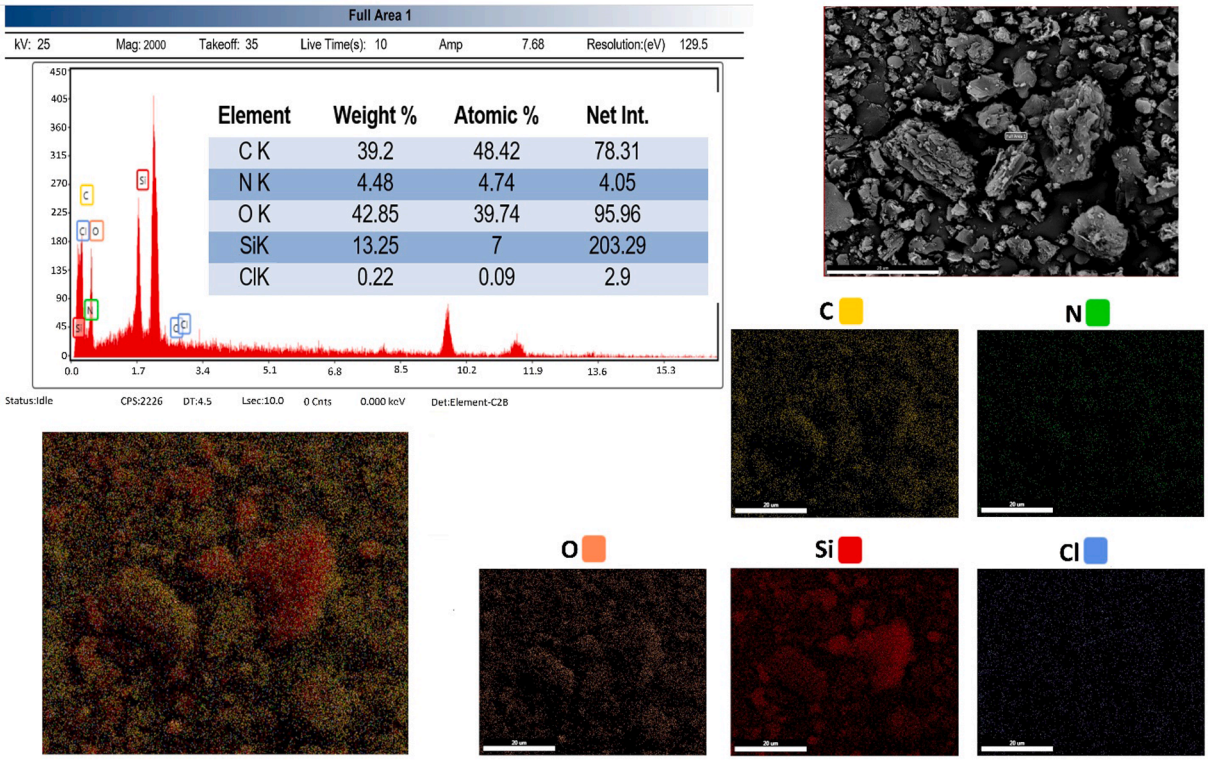

Fig. 7. EDX mapping analysis of FGO-POSS.

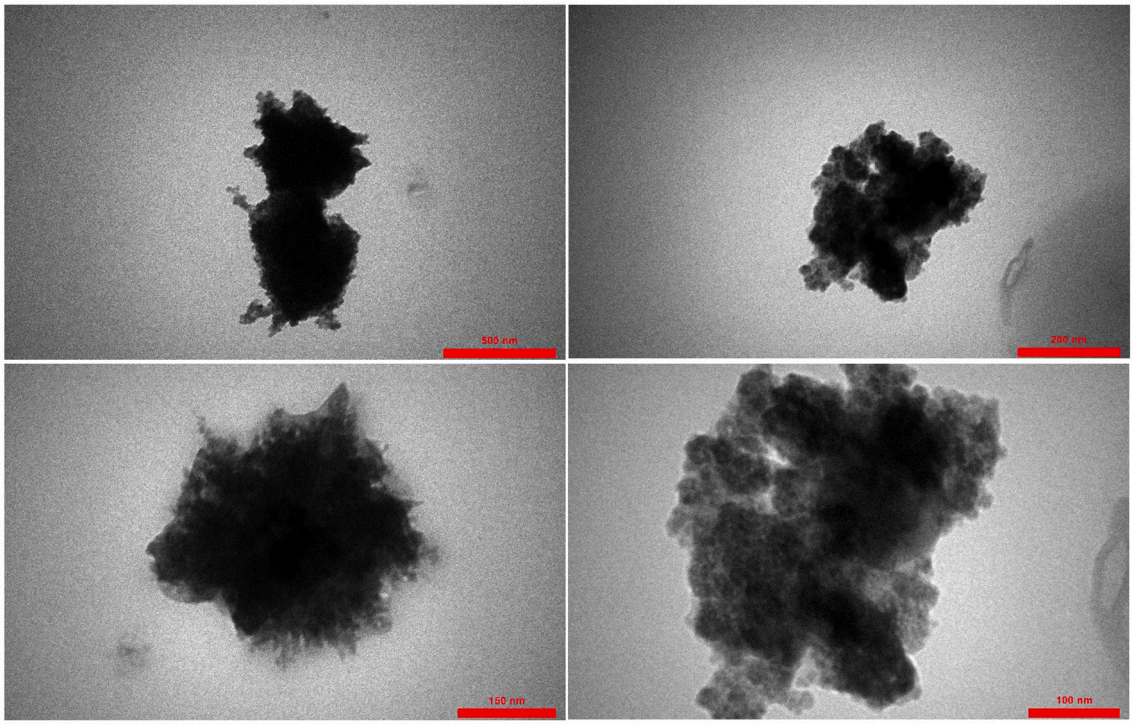

Fig. 8. TEM images of FGO-POSS.

characteristics of GO, which illustrates GO's layered structure. The intensity of this wrinkle increased after GO functionalization, which is due to a decrease in the spacing between GO sheets following functionalization. According to the images obtained, GO has preserved its porous and spongy state after being functionalized with POSS [62,66].

The stoichiometric ratio of the material composition as well as the elemental analysis of the surface of the synthesized material can be seen in the energy-dispersive X-ray (EDS) mapping FGO-POSS images in Fig. 7. The atomic percentages of five elements in EDS analysis are such that the highest atomic percentages for carbon, oxygen, silicon, nitrogen, and chlorine elements are 48.42 %, 39.74 %, 7 %, 4.74 %, and 0.09 %, respectively. It should be mentioned that the presence of oxygen with

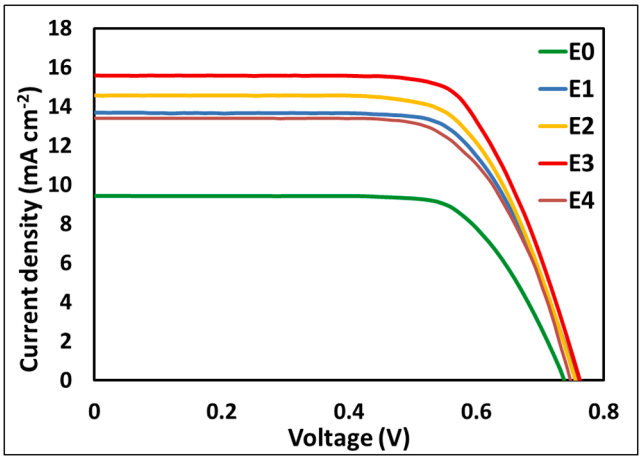

Fig. 9. Current density–voltage characteristic curve (J-V) of DSSCs with standard electrolyte E0 and nanocomposite electrolytes E1, E2, E3, and E4.

Table 2
Photovoltaic characteristics of DSSCs fabricated with nanocomposite electrolytes E1, E2, E3, and E4 (varying percentages of FGO-POSS) and standard electrolyte E0.

Cells (FGO-POSS wt. %)	J_{SC}[mA.cm^{-2}]	V_{OC}[V]	η[%]	FF
E0 (0 wt%)	9.433	0.738	4.965	0.713
E1 (0.25 wt%)	13.694	0.758	7.169	0.691
E2 (0.5 wt%)	14.576	0.755	7.574	0.688
E3 (0.75 wt%)	15.592	0.762	8.303	0.699
E4 (1 wt%)	13.407	0.748	6.877	0.686

Table 3
EIS parameters derived by using ZView software to fit experimental data.

Cells	R_S (Ω)	R_1 (Ω)	R_2 (Ω)	R_{Diff} (Ω)
E0 (Standard electrolyte)	20.43	17.12	63.54	72.15
E3 (0.75 wt% FGO-POSS)	13.09	6.39	18.43	27.16

the most significant percentage by weight has to do with including this element in the structure of GO and POSS.

Transmission electron microscopy (TEM) imaging has been utilized to investigate the morphology of the FGO-POSS (Fig. 8). Because the epoxy, hydroxyl, and carboxyl groups bonded to the GO surface, the TEM picture of FGO-POSS shows a smooth and wavy structure. The covalent bonding of GO with POSS after functionalization has resulted in a relatively rough surface for FGO. As a result of the characteristics mentioned about FGO-POSS, it can be stated that the surface of GO has been modified utilizing POSS, and as a result, our functionalization procedure has been successful [67,68].

3.2. The DSSC's photovoltaic efficiency employing nanocomposite electrolytes

The photovoltaic efficiency of ionic liquid-based DSSCs employing EMII and $BMICuI_2$ was researched and assessed by preparing nanocomposite electrolytes E1, E2, E3, E4, and a standard electrolyte E0. The results of this comparison are shown in Fig. 9 as Diagram IV, and their values are given in Table 2. According to the photovoltaic properties and results of DSSCs, FGO-POSS's presence in the nanocomposite's electrolytes has enhanced the DSSCs' efficiency compared to standard electrolyte without graphene composition. Compared to DSSCs using an E0 electrolyte, the efficiency of DSSCs employing an E1 electrolyte, which contains 0.25 wt% FGO-POSS, has risen from 4.965 to 7.169 %. This efficiency boost is due to the addition of FGO-POSS to the DSSC's electrolyte structure. Due to the properties of POSS and graphene, this effective additive in the electrolyte composition improves electron transfers and, as a result, the conductivity of the electrolyte and speeds up the I^-/I_3^- redox process. POSS has a nanostructure, is polyhedral, and has a unique dual nature that combines the properties of inorganic siloxane cage materials and organic groups. Also, the unique properties of graphene have enabled FGO-POSS to serve as a molecular bridge to enhance electron transmission in DSSC electrolytes. By adding up to 0.75 wt% FGO-POSS to the electrolyte composition of DSSCs, the efficiency (η) of DSSCs is increased by boosting the amount of open circuit voltage (V_{OC}) and short circuit current (J_{SC}). Incorporating 1 wt% FGO-POSS to the electrolyte composition in E4 reduces the value of V_{OC} and J_{SC}, leading to a decrease in efficiency when compared to the E3 electrolyte. As the amount of FGO-POSS grows up to 1 wt%, the viscosity of the electrolyte rises, and electron transport diminishes, causing the efficiency of DSSCs to fall. The value of FF in DSSCs with nanocomposite electrolytes is affected by the rise in viscosity, and its value drops when compared to DSSCs with standard electrolytes, which is the reverse of the upward trend in DSSCs' efficiency while using nanocomposite electrolytes. According to the results, the significant effect of FGO-POSS as an innovative and efficient additive in enhancing the efficiency of DSSCs using E1, E2, E3, and E4 electrolytes is due to the unique

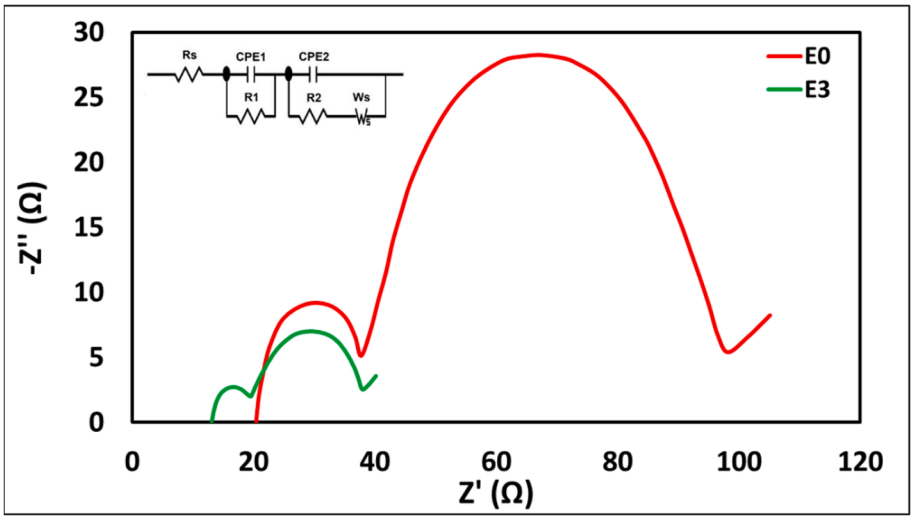

Fig. 10. EIS spectrum of DSSCs with E3 nanocomposite electrolyte and E0 standard electrolyte.

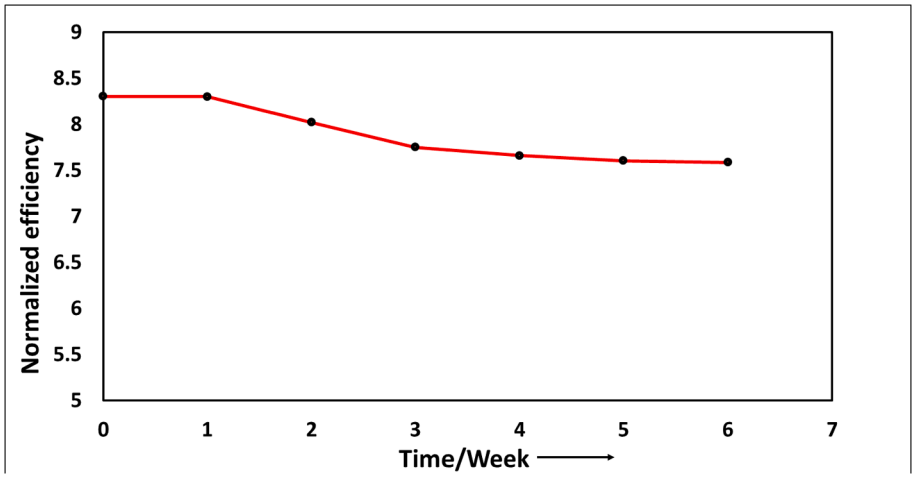

Fig. 11. Long-term variations in the normalized efficiency of the DSSC using the E3 electrolyte.

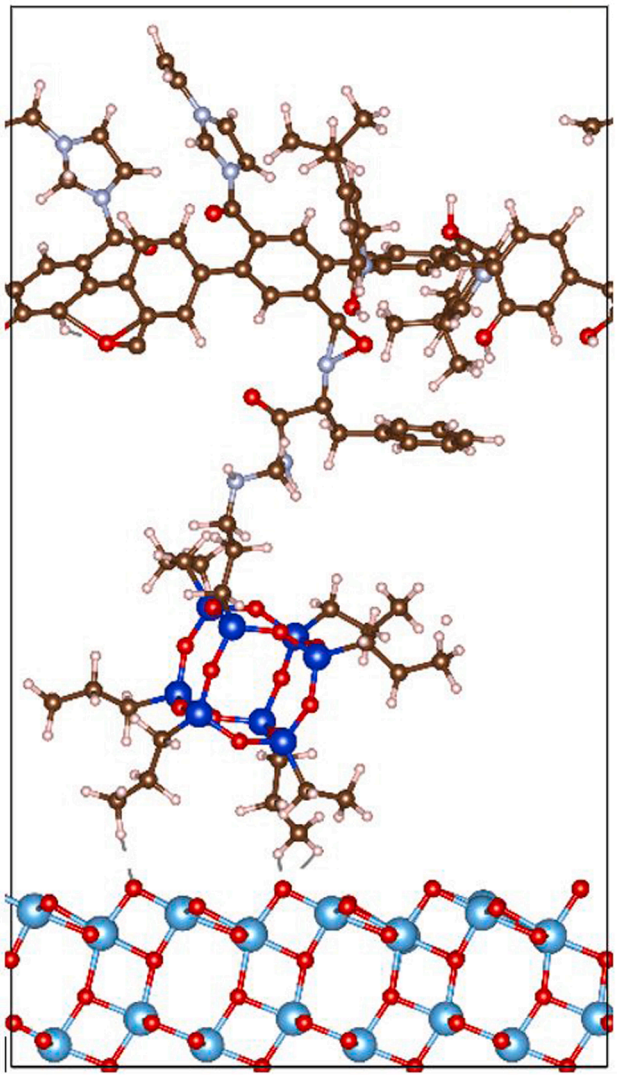

Fig. 12. The adsorption structure of the FGO-POSS incorporated with ILs and TBPs on anatase TiO_2 (101) surface is depicted. In the illustration, brown spheres are used to represent carbon atoms, oxygen atoms by red spheres, titanium atoms by larger blue spheres, nitrogen atoms by smaller blue spheres, and hydrogen atoms by white spheres.

properties of this synthesized material. Compared to functionalized graphene oxides with transition metal complexes and polymer electrolytes based on functionalized ionic liquids with POSS, the application of FGO-POSS as an effective additive in the electrolyte based on EMII and $BMICuI_2^-$ ionic liquids for the first time offers an attractive and competitive concept.

3.3. Electrochemical performances of DSSCs

In this analysis, four parameters (R_S, R_1, R_2, and R_{Diff}) were assessed for two different DSSC variants using E0 and E3 electrolytes, according to the EIS (Electrochemical Impedance Spectroscopy) parameters presented in Table 3. R_S stands for series resistance, R_1 is the resistance associated with the cathode, R_2 is the resistance produced by TiO_2/electrolyte/dye, and R_{Diff} is the Warburg resistance, which is related to the diffusion process (I^-/I_3^-) in the electrolyte. In DSSCs with E3 nanocomposite electrolyte, the resistances R_S, R_1, R_2, and R_{Diff} have all significantly decreased in comparison with standard electrolyte, given the data found in Table 3 and shown in Fig. 10. The inclusion of effective additive FGO-POSS in the electrolyte structure of DSSCs can be attributed to the decrease in resistance. FGO-POSS works as a molecular bridge for electron transport inside the electrolyte, and it, together with (Cu^{2+}/Cu^+), participates in the (I^-/I_3^-) redox reactions and speeds up the oxidation–reduction and dye regeneration processes. In general, the performance of these solar cells has been significantly impacted by the use of FGO-POSS as an innovative and efficient additive in DSSC electrolytes.

3.4. Long-term stability

An ageing test at 60 °C for 1008 h was used to examine the long-term cell stability of DSSC with E3 electrolyte, which exhibited the best efficiency among all DSSCs. Fig. 11 displays the results related to the cell efficiency measurement during 1008 h, which were measured each week under the same conditions. The stability of DSSC has remained at 91 % after 1008 h. This indicates that the presence of FGO-POSS in the electrolyte structure of DSSC has prevented electrolyte leakage and has long-term maintained the electrolyte's conductivity [17,33].

3.5. Computational calculations

3.5.1. DFT method

To gain further insight into the impact of incorporating FGO-POSS as an additive to the standard electrolyte of DSSC, the researchers conducted density functional theory (DFT) calculations [69,70]. These calculations aimed to investigate the electronic properties of the

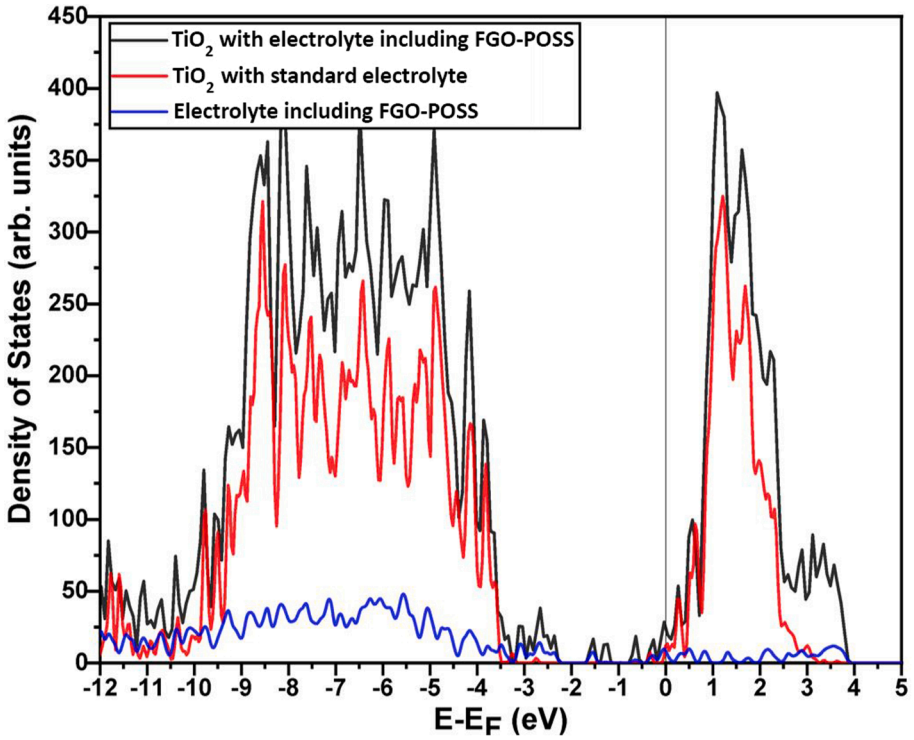

Fig. 13. The density of states was computed for the adsorption configuration of the FGO-POSS with ILs and TBPs on the surface of anatase TiO_2 (1 0 1). The calculated density of states indicates the energy distribution of electronic states within the system, with the Fermi level located at 0 eV.

interface between the TiO_2 electrode and the electrolyte. The Vienna ab initio simulation package (VASP)[71,72] was employed, which utilizes a plane-wave basis set and the generalized gradient approximation (GGA) [73] with the Perdew-Burke-Ernzerhof (PBE) functional [74] and projected-augmented wave (PAW)[75] method.

For the electronic properties calculations, the PBE0 hybrid functional [76–78] was utilized, and the Grimme Scheme [79] was employed to account for dispersion correction. The expansion of the plane wave basis sets and the sampling of the Brillouin zone were performed using a cutoff energy of 500 eV and a Γ point grid of the Monkhorst Pack scheme [80], respectively. During the geometry optimization, convergence criteria were set at 0.01 eV/Å for energy and 10–5 eV for the maximum force on atoms.

3.5.2. *DFT model*

Fig. 12 illustrates the interface between the TiO_2 surface, serving as the electrode, and FGO-POSS in the presence of IL (ionic liquid) and TBPs (*tert*-butylpyridine) as the electrolyte. The stable anatase TiO_2 (1 0 1) facet [81–83] was utilized, with calculated lattice constants of a and b equal to 3.784 Å and c equal to 9.514 Å, consistent with experimental values [84]. The TiO_2 (1 0 1) surface consisted of a fixed bottom layer and four relaxed layers on top, as per previous literature [85].

To simulate the electrolyte component of the system, a GO layer containing hydroxyl and carboxyl functional groups at the edges was constructed. Subsequently, IL and TBP molecules, representing the base electrolyte, and POSS as the additive, were introduced onto the GO layer to examine their interactions with the TiO_2 surface, as depicted in Fig. 12.

3.5.3. *DFT results*

Fig. 13 presents the overall density of states for the nanocomposite system, specifically the adsorption arrangement of the FGO-POSS integrated with ILs and TBPs, which constitute the standard electrolyte, on the anatase TiO_2 (1 0 1) surface. The findings indicate that the incorporation of FGO-POSS as a potential additive generates intermediate states within the band gap of the nanocomposite, which are absent in the band gap of TiO_2 with the standard electrolyte. This outcome leads to an enhancement in the efficiency of DSSCs by augmenting composite conductivity and facilitating electron transfer across the interface between TiO_2 and the electrolyte.

4. Conclusions

This study marked the first application of FGO-POSS as a novel and effective additive in IL-based electrolytes for DSSCs, which increased the efficiency of DSSCs. Furthermore, synthesizing IL with imidazolium cation and CuI_2^- anion and their use in DSSC electrolytes instead of organic solvents increase DSSC stability and efficiency by boosting conductivity and decreasing electrolyte leakage. Because of the characteristics of POSS and the presence of this compound in the structure of the graphene compound, functionalization of GO with POSS improves the conductivity properties of the graphene compound while also increasing electron transport in DSSCs electrolytes and thus increasing efficiency. Utilizing the optimal amount of 0.75 wt%.

FGO-POSS in electrolytes based on EMII and $BMICuI_2^-$ ionic liquids boosted efficiency by 67.23 % from 4.965 to 8.303 when compared to DSSCs with standard electrolytes without FGO-POSS. As a result, FGO-POSS in ionic liquid-based electrolytes increases the rate of the I^-/I_3^- redox reaction by enhancing electron transfer and electrolyte conductivity, hence raising the amount of VOC, JSC, and efficiency of DSSCs. DFT calculations showed the appearance of a number of midgap states in the TiO_2 bandgap due to adding the FGO-POSS as the new additive to the standard electrolyte leading to increasing composite conductivity and the efficiency of DSSCs.

CRediT authorship contribution statement

Shiva Orangi: Data curation, Formal analysis, Investigation, Methodology, Writing – original draft, Writing – review & editing. **Elaheh Kowsari:** Conceptualization, Funding acquisition, Investigation,

Methodology, Project administration, Supervision, Writing – review & editing. **Mohammad Mohammadizadeh Boghrabad:** Investigation, Methodology, Writing – original draft, Writing – review & editing. **Saeedeh Sarabadani Tafreshi:** Methodology, Visualization, Writing – review & editing. **Seeram Ramakrishna:** Conceptualization, Writing – review & editing, Project administration, Funding acquisition. **Mahboobeh Rafieepoor Chirani:** Data curation, Formal analysis, Writing – review & editing. **Amutha Chinnappan:** Data curation, Formal analysis, Writing – review & editing. **Nora H. de Leeuw:** Funding acquisition, Methodology, Software, Writing – review & editing.

Declaration of competing interest

The authors declare that they have no known competing financial interests or personal relationships that could have appeared to influence the work reported in this paper.

Data availability

Data will be made available on request.

Acknowledgments

The Amirkabir University of Technology (AUT), located in Tehran, Iran, provided the authors of this article with financial support, which they gratefully acknowledge. The IAFPP project A-0009465-05-00 “Sustainable Tropical Data Centre Test Bed” funded by the National Research Foundation of Singapore, is acknowledged by authors. This project made use of the ARCHER2 UK National Supercomputing Service (http://archer2.ac.uk) through our participation in the UK’s HEC Materials Chemistry Consortium, sponsored by the EPSRC (EP/R029431). Additionally, this project utilized computational resources made available by Cardiff University, HPC Wales, and the Advanced Research Computing at Cardiff (ARCCA) Division.

References

[1] M.A. Agoro, E.L. Meyer, J.Z. Mbese, K. Manu, Electrochemical fingerprint of CuS-hexagonal chemistry from (Bis (N-1, 4-Phenyl-N-(4-morpholinedithiocarbamato) copper (II) complexes) as photon absorber in quantum-dot/dye-sensitised solar cells, Catalysts 10 (3) (2020) 300.
[2] G. Boschloo, Improving the performance of dye-sensitized solar cells, Front. Chem. 7 (2019) 77.
[3] N. Kannan, D. Vakeesan, Solar energy for future world:-A review, Renew. Sustain. Energy Rev. 62 (2016) 1092–1105.
[4] L. Matović, et al., Synthesis of novel pyridinium based compounds and their possible application in dye-sensitized solar cells, J. Mol. Struct. 1274 (2023) 134433.
[5] N. Wazzan, A. Irfan, T.M. Fagieh, DFT investigation of graphene quantum dot-Ixora floral natural dye (GQD-NDIX) nanocomposites as visible light harvesters in dye-sensitized solar cells, J. Mol. Liq. 360 (2022) 119531.
[6] M.R. Al-Mamun, et al., State-of-the-art in solar water heating (SWH) systems for sustainable solar energy utilization: A comprehensive review, Sol. Energy (2023) 111998.
[7] J. Gong, K. Sumathy, Q. Qiao, Z. Zhou, Review on dye-sensitized solar cells (DSSCs): Advanced techniques and research trends, Renew. Sustain. Energy Rev. 68 (2017) 234–246.
[8] S. Kumar, et al., Recent development in two-dimensional material-based advanced photoanodes for high-performance dye-sensitized solar cells, Sol. Energy 249 (2023) 606–623.
[9] T. Ghaed-Sharaf, A. Omidvar, Charge transport through molecular ensembles: Triphenylamine-based organic dyes, J. Mol. Liq. (2023) 122304.
[10] R. Senthilkumar, et al., CoxMo (1–x) S2 intermixed reduced graphene oxide as efficient counter electrode materials for high-performance dye-sensitized solar cells, Int. J. Hydrogen Energy 48 (15) (2023) 5901–5914.
[11] W. Mao, L. Wei, X. Xu, L. Zhao, J. Liu, Z. Zhang, One-step hydrothermal preparation of bi-functional NiS2/reduced graphene oxide composite electrode material for dye-sensitized solar cells and supercapacitors, Int. J. Hydrogen Energy (2023).
[12] B. O’regan, M. Grätzel, A low-cost, high-efficiency solar cell based on dye-sensitized colloidal TiO2 films, Nature 353 (6346) (1991) 737–740.
[13] Z.-S. Wu, et al., Effects of side substituents in bithiophene spacer on the performance of dye-sensitized solar cells with cobalt electrolyte, Sol. Energy 218 (2021) 503–511.
[14] B. Lin, et al., Ionic liquid-tethered graphene oxide/ionic liquid electrolytes for highly efficient dye sensitized solar cells, Electrochim. Acta 134 (2014) 209–214.
[15] Y. Ren, et al., Hydroxamic acid pre-adsorption raises the efficiency of cosensitized solar cells, Nature 613 (7942) (2023) 60–65.
[16] P. Manafi, H. Nazockdast, M. Karimi, M. Sadighi, L. Magagnin, A study on the microstructural development of gel polymer electrolytes and different imidazolium-based ionic liquids for dye-sensitized solar cells, J. Power Sources 481 (2021) 228622.
[17] M.R. Chirani, E. Kowsari, H. SalarAmoli, M. Yousefzadeh, A. Chinnappan, S. Ramakrishna, Covalently functionalized graphene oxide with cobalt–nitrogen-enriched complex containing iodide ligand as charge carrier nanofiller for eco-friendly high performance ionic liquid-based dye-sensitized solar cell, J. Mol. Liq. 325 (2021) 115198.
[18] Masud, H.K. Kim, Redox shuttle-based electrolytes for dye-sensitized solar cells: comprehensive guidance, recent progress, and future perspective, ACS Omega 8 (7) (2023) 6139–6163.
[19] J. Wu, P. Li, S. Hao, H. Yang, Z. Lan, A polyblend electrolyte (PVP/PEG+ KI+ I2) for dye-sensitized nanocrystalline TiO2 solar cells, Electrochim. Acta 52 (17) (2007) 5334–5338.
[20] S. Peng, et al., Platinum/polyaniline transparent counter electrodes for quasi-solid dye-sensitized solar cells with electrospun PVDF-HFP/TiO2 membrane electrolyte, Electrochim. Acta 105 (2013) 447–454.
[21] R. Atasiei, M. Raicopol, C. Andronescu, A. Hanganu, A. Alexe-Ionescu, G. Barbero, Investigation of the conduction properties of ionic liquid crystal electrolyte used in dye sensitized solar cells, J. Mol. Liq. 267 (2018) 81–88.
[22] E. Kowsari, M.R. Chirani, High efficiency dye-sensitized solar cells with tetra alkyl ammonium cation-based ionic liquid functionalized graphene oxide as a novel additive in nanocomposite electrolyte, Carbon 118 (2017) 384–392.
[23] N.I.M.F. Hilmy, W.Z.N. Yahya, K.A. Kurnia, Eutectic ionic liquids as potential electrolytes in dye-sensitized solar cells: Physicochemical and conductivity studies, J. Mol. Liq. 320 (2020) 114381.
[24] G. Choudhary, et al., Ionic liquids: environmentally sustainable materials for energy conversion and storage applications, Environ. Sci. Pollut. Res. (2023) 1–21.
[25] T. Sharma, et al., Ionic liquid doped Poly (methyl methacrylate) for energy applications, J. Mol. Liq. 352 (2022) 118494.
[26] G. Kaur, H. Kumar, M. Singla, Diverse applications of ionic liquids: A comprehensive review, J. Mol. Liq. (2022) 118556.
[27] J. Siavashi, A. Najafi, A. Moslemizadeh, M. Sharifi, E. Kowsari, S. Zendehboudi, Design and synthesis of a new ionic liquid surfactant for petroleum industry, J. Mol. Liq. 367 (2022) 120047.
[28] A.R. Zolghadr, N. Azari, M.H. Dokoohaki, The use of 1-ethyl-3-methylimidazolium iodide ionic liquid in dye sensitized solar cells: A joint experimental and computational perspective, J. Mol. Liq. 364 (2022) 119982.
[29] D. Gurina, E. Odintsova, M. Krestianinov, Y. Budkov, Transport properties of imidazolium-based room temperature ionic liquids in confinement of slit charged carbon nanopores: New insights from molecular simulations, J. Mol. Liq. 390 (2023) 122961.
[30] K. Srivishnu, S. Prasanthkumar, L. Giribabu, Cu (II/I) redox couples: Potential alternatives to traditional electrolytes for dye-sensitized solar cells, Mater. Adv. 2 (4) (2021) 1229–1247.
[31] M. Kandhasamy, G. Shanmugam, S. Kamaraj, B. Selvaraj, A. Gunasekeran, A. Sambandam, Effect of D-limonene additive in copper redox-based quasi-solid-state electrolytes on the performance of dye-sensitized solar cells, Mater. Today Commun. 35 (2023) 105505.
[32] A.K. Bharwal, et al., Remarkable 8.3% efficiency and extended electron lifetime towards highly stable semi-transparent iodine-free DSSCs by mitigating the in-situ triiodide generation, Chem. Eng. J. 446 (2022) 136777.
[33] S. Venkatesan, E. Surya Darlim, M.-H. Tsai, H. Teng, Y.-L. Lee, Graphene oxide sponge as nanofillers in printable electrolytes in high-performance quasi-solid-state dye-sensitized solar cells, ACS Appl. Mater. Interfaces 10 (13) (2018) 10955–10964.
[34] K. Susmitha, et al., Carbon nanohorns based counter electrodes developed by spray method for dye sensitized solar cells, Sol. Energy 133 (2016) 524–532.
[35] P.D. Adhikari, Y.-H. Ko, D. Jung, C.-Y. Park, Single-wall carbon nanotube hybridized graphene films: self assembly and electrical properties, New Carbon Mater. 30 (4) (2015) 342–348.
[36] H. Im, J. Kim, Thermal conductivity of a graphene oxide–carbon nanotube hybrid/epoxy composite, Carbon 50 (15) (2012) 5429–5440.
[37] A.A. Ashtiani, et al., Pseudocapacitive efficiency of covalently Cr-complex with L-histidine-methyl ester as a ligand graphene oxide blended with conducting polymer (POAP) as electrode material in supercapacitor, J. Mol. Liq. 315 (2020) 113697.
[38] F. Shoushtarian, M.R.A. Moghaddam, E. Kowsari, Efficient regeneration/reuse of graphene oxide as a nanoadsorbent for removing basic Red 46 from aqueous solutions, J. Mol. Liq. 312 (2020) 113386.
[39] E. Kowsari, A. Zare, V. Ansari, Phosphoric acid-doped ionic liquid-functionalized graphene oxide/sulfonated polyimide composites as proton exchange membrane, Int. J. Hydrogen Energy 40 (40) (2015) 13964–13978.
[40] H. Esmaili, E. Kowsari, S.S. Tafreshi, S. Ramakrishna, N.H. de Leeuw, M. Abdouss, TiO2 nanoarrays modification by a novel Cobalt-heteroatom doped graphene complex for photoelectrochemical water splitting: An experimental and theoretical study, J. Mol. Liq. 356 (2022) 118960.
[41] H. Su, Y.H. Hu, 3D graphene: synthesis, properties, and solar cell applications, Chem. Commun. (2023).

[42] C. Prasad, et al., An overview of graphene oxide supported semiconductors based photocatalysts: Properties, synthesis and photocatalytic applications, J. Mol. Liq. 297 (2020) 111826.
[43] N. Kumar, A. Kozakov, A. Sidashov, A. Nicolskii, Tribofilm stability of ionic liquid functionalized graphene-oxide in metallic contact interfaces, J. Mol. Liq. 296 (2019) 111813.
[44] M.M. Boghrabad, et al., A novel smart framework for sustainable nanocomposite electrolytes based on ionic liquids of dye-sensitized solar cells by a covalently multifunctional graphene oxide-vinyl imidazole/4-tert-butylpyridine cobalt complex, J. Alloy. Compd. 945 (2023) 169241.
[45] M.D. Najafi, et al., High-performance symmetric supercapacitor based on new functionalized graphene oxide composites with pyrimidine nucleotide and nucleoside, J. Mol. Liq. 348 (2022) 118381.
[46] M.D. Najafi, et al., TMP/Pd complex immobilized on graphene oxide for efficient pseudocapacitive energy storage with combined experimental and DFT study, J. Mol. Liq. 364 (2022) 120008.
[47] D. Raja, B. Selvaraj, G. Shanmugam, A. Maruthapillai, D. Sundaramurthy, Improving the efficiency of dye-sensitized solar cells via the impact of triphenylamine-based inventive organic additives on biodegradable cellulose polymer gel electrolytes, Energy Fuel 35 (5) (2021) 4273–4282.
[48] J. Abisharani, R. Dineshkumar, S. Devikala, M. Arthanareeswari, S. Ganesan, Influence of 2, 4-Diamino-6-Phenyl-1-3-5-triazine on bio synthesized TiO2 dye-sensitized solar cell fabricated using poly (ethylene glycol) polymer electrolyte, Mater. Res. Express 7 (2) (2020) 025507.
[49] R. Aliakbari, E. Kowsari, H.R. Naderi, S. Ramakrishna, A. Chinnappan, M.D. Najafi, N-heterocycle-functionalized graphene oxide complexed with cobalt (II) as symmetric supercapacitor electrodes, J. Alloy. Compd. 914 (2022) 165371.
[50] M. D. Najafi, E. Kowsari, S. Ramakrishna, and R. AliAkbari, "Functionalization of graphene composites using ionic liquids and applications," in *Innovations in Graphene-Based Polymer Composites*: Elsevier, 2022, pp. 445-461.
[51] K. Rajavelu, M. Sudip, R. Kothandaraman, P. Rajakumar, Synthesis and DSSC application of triazole bridged dendrimers with benzoheterazole surface groups, Sol. Energy 166 (2018) 379–389.
[52] K. Lv, W. Zhang, L. Zhang, Z.-S. Wang, POSS-based electrolyte for efficient solid-state dye-sensitized solar cells at sub-zero temperatures, ACS Appl. Mater. Interfaces 8 (8) (2016) 5343–5350.
[53] M. Čolović, J. Volavšek, E. Stathatos, N.Č. Korošin, M. Šobak, I. Jerman, Amphiphilic POSS-based ionic liquid electrolyte additives as a boost for dye-sensitized solar cell performance, Sol. Energy 183 (2019) 619–631.
[54] F. Sun, et al., Large-Area Flexible Electrochromic Devices with High-Performance and Low-Power Consumption Enabled by Hydroxyhexyl Viologen-Substituted Polyhedral Oligomeric Silsesquioxane, ACS Sustain. Chem. Eng. 11 (14) (2023) 5756–5763.
[55] T.-Y. Cho, S.-G. Yoon, S. Sekhon, C.-H. Han, Effect of Ionic Liquids with Different Cations in I−/I3− Redox Electrolyte on the Performance of Dye-sensitized Solar Cells, Bull. Korean Chem. Soc. 32 (2011) 2058–2062.
[56] S. William, J. Hummers, R.E. Offeman, Preparation of graphitic oxide, J. Am. Chem. Soc 80 (6) (1958) 1339.
[57] F. Saltan, H. Akat, Y. Yıldırım, Synthesis and characterization of the POSS/PCL-graphene oxide composites; the effects of gamma-radiation on its thermal properties and molecular weight, Mater. Res. Express 6 (12) (2019) 125328.
[58] Z. Teng, B. Wang, Y. Hu, D. Xu, Light-responsive nanocomposites combining graphene oxide with POSS based on host-guest chemistry, Chin. Chem. Lett. 30 (3) (2019) 717–720.
[59] M. Mohamadi, E. Kowsari, V. Haddadi-Asl, M. Yousefzadeh, Fabrication, characterization and electromagnetic wave absorption properties of covalently modified reduced graphene oxide based on dinuclear cobalt complex, Compos. B Eng. 162 (2019) 569–579.
[60] Y. Xue, Y. Liu, F. Lu, J. Qu, H. Chen, L. Dai, Functionalization of graphene oxide with polyhedral oligomeric silsesquioxane (POSS) for multifunctional applications, J. Phys. Chem. Lett. 3 (12) (2012) 1607–1612.
[61] A.M. Joseph, B. Nagendra, K. Surendran, E.B. Gowd, Sustainable in situ approach to covalently functionalize graphene oxide with POSS molecules possessing extremely low dielectric behavior, Langmuir 35 (13) (2019) 4672–4681.
[62] M. Namvari, L. Du, F.J. Stadler, Graphene oxide-based silsesquioxane-crosslinked networks–synthesis and rheological behavior, RSC Adv. 7 (35) (2017) 21531–21540.
[63] X. Du, Y. Liu, Y. Chen, Enhancing the corrosion resistance of aluminum by superhydrophobic silane/graphene oxide coating, Appl. Phys. A 127 (2021) 1–11.
[64] H. Jiang, Y. Ji, J. Gan, L. Wang, Enhancement of thermal and mechanical properties of bismaleimide using a graphene oxide modified by epoxy silane, Materials 13 (17) (2020) 3836.
[65] M.R. Chirani, E. Kowsari, S. Ramakrishna, H.S. Amoli, M. Yousefzadeh, A. Chinnappan, A sustainable gel-state ionic liquid-based dye-sensitized solar cell with a novel synthesized lansoprazole functionalized graphene oxide, J. Mol. Liq. 364 (2022) 119999.
[66] A. Dimiev, D.V. Kosynkin, L.B. Alemany, P. Chaguine, J.M. Tour, Pristine graphite oxide, J. Am. Chem. Soc. 134 (5) (2012) 2815–2822.
[67] N. Divakaran, et al., Novel unsaturated polyester nanocomposites via hybrid 3D POSS-modified graphene oxide reinforcement: electro-technical application perspective, Nanomaterials 10 (2) (2020) 260.
[68] W.-H. Liao, et al., Effect of octa (aminophenyl) polyhedral oligomeric silsesquioxane functionalized graphene oxide on the mechanical and dielectric properties of polyimide composites, ACS Appl. Mater. Interfaces 6 (18) (2014) 15802–15812.
[69] P. Hohenberg, W. Kohn, Inhomogeneous electron gas, Phys. Rev. 136 (3B) (1964) B864.
[70] W. Kohn, L.J. Sham, Self-consistent equations including exchange and correlation effects, Phys. Rev. 140 (4A) (1965) A1133.
[71] G. Kresse, J. Furthmüller, Efficiency of ab-initio total energy calculations for metals and semiconductors using a plane-wave basis set, Comput. Mater. Sci 6 (1) (1996) 15–50.
[72] G. Kresse, J. Furthmüller, "Efficient iterative schemes for ab initio total-energy calculations using a plane-wave basis set, Phys. Rev. B 54 (1996) 11169–11186.
[73] J.P. Perdew, K. Burke, M. Ernzerhof, Generalized gradient approximation made simple, Phys. Rev. Lett. 77 (18) (1996) 3865.
[74] J. Paier, R. Hirschl, M. Marsman, G. Kresse, The Perdew–Burke–Ernzerhof exchange-correlation functional applied to the G2–1 test set using a plane-wave basis set, J. Chem. Phys. 122 (23) (2005) 234102.
[75] P.E. Blöchl, Projector augmented-wave method, Phys. Rev. B 50 (24) (1994) 17953.
[76] M. Ernzerhof, G.E. Scuseria, Assessment of the Perdew–Burke–Ernzerhof exchange-correlation functional, J. Chem. Phys. 110 (11) (1999) 5029–5036.
[77] C. Adamo, V. Barone, Toward reliable density functional methods without adjustable parameters: The PBE0 model, J. Chem. Phys. 110 (13) (1999) 6158–6170.
[78] J.P. Perdew, M. Ernzerhof, K. Burke, Rationale for mixing exact exchange with density functional approximations, J. Chem. Phys. 105 (22) (1996) 9982–9985.
[79] S. Grimme, S. Ehrlich, L. Goerigk, Effect of the damping function in dispersion corrected density functional theory, J. Comput. Chem. 32 (7) (2011) 1456–1465.
[80] H.J. Monkhorst, J.D. Pack, Special points for Brillouin-zone integrations, Phys. Rev. B 13 (12) (1976) 5188.
[81] M. Lazzeri, A. Vittadini, A. Selloni, Structure and energetics of stoichiometric TiO 2 anatase surfaces, Phys. Rev. B 63 (15) (2001) 155409.
[82] Y. Jiao, F. Zhang, M. Grätzel, S. Meng, Structure–Property Relations in All-Organic Dye-Sensitized Solar Cells, Adv. Funct. Mater. 23 (4) (2013) 424–429.
[83] H.G. Yang, et al., Anatase TiO2 single crystals with a large percentage of reactive facets, Nature 453 (7195) (2008) 638–641.
[84] J.K. Burdett, T. Hughbanks, G.J. Miller, J.W. Richardson Jr, J.V. Smith, Structural-electronic relationships in inorganic solids: powder neutron diffraction studies of the rutile and anatase polymorphs of titanium dioxide at 15 and 295 K, J. Am. Chem. Soc. 109 (12) (1987) 3639–3646.
[85] W. Orellana, D-π-A dye attached on TiO2 (101) and TiO2 (001) surfaces: Electron transfer properties from ab initio calculations, Sol. Energy 216 (2021) 266–273.